Check for updates

Predicting lung cancer's metastats' locations using bioclinical model

Teddy Lazebnik[1,2] and Svetlana Bunimovich-Mendrazitsky[2]*

[1]Department of Cancer Biology, Cancer Institute, University College London, London, United Kingdom, [2]Department of Mathematics, Ariel University, Ariel, Israel

Background: Lung cancer is a global leading cause of cancer-related deaths, and metastasis profoundly influences treatment outcomes. The limitations of conventional imaging in detecting small metastases highlight the crucial need for advanced diagnostic approaches.

Methods: This study developed a bioclinical model using three-dimensional CT scans to predict the spatial spread of lung cancer metastasis. Utilizing a three-layer biological model, we identified regions with a high probability of metastasis colonization and validated the model on real-world data from 10 patients.

Findings: The validated bioclinical model demonstrated a promising 74% accuracy in predicting metastasis locations, showcasing the potential of integrating biophysical and machine learning models. These findings underscore the significance of a more comprehensive approach to lung cancer diagnosis and treatment.

Interpretation: This study's integration of biophysical and machine learning models contributes to advancing lung cancer diagnosis and treatment, providing nuanced insights for informed decision-making.

1 Background

Treating cancer is a critical challenge in modern medicine, as it affects millions of people worldwide and can have devastating effects on both patient health and quality of life. Lung cancer, in particular, is one of the most prevalent and deadly forms of cancer worldwide (1). One of the major challenges in treating lung cancer is the development of metastases, which are secondary tumors that develop from cells that have spread from the primary tumor site to other parts of the organ (or even the body) (2–4). The location of these metastases can greatly affect a patient's prognosis and the effectiveness of treatment (5).

In particular, for lung cancer diagnosis, healthcare professionals commonly use a *computed tomography* (CT) and Positron Emission Tomography CT (PET-CT) to diagnose the patient's clinical condition (6, 7). This non-invasive imaging modality allows for the simultaneous acquisition of functional and anatomic information, providing detailed insights into the metabolic activity of the tumor and its relationship to surrounding tissue. Additionally, this analysis provides the anatomy and structure of the lung and surrounding tissue, which can be used to determine the size and location of the tumor. Based on this data, clinicians look for the primary cancer tumor's as well as metastasis' properties to determine the course of treatment (8–10).

Recently, to partially automate the process of parsing the required clinical data from CT imagery, researchers have used computer vision and ML algorithms in general and to detect lung cancer, in particular (11–14). These algorithms can (semi-)automatically detect and classify lung nodules, reducing the dependence on human interpretation and improving the consistency of diagnoses. In addition, biophysical models gathering popularity in the clinical domain as these getting better at predicting clinical outcomes over time (15–19). For instance, Kang et al. (20) constructs a mathematical model that integrates let-7 and miR-9 expression into a signaling pathway to generate an *in silico* model for the process of epithelial-mesenchymal transition. The authors validate their model using *in vitro* data collected by testing the effects of EGFR inhibition on downstream MYC, miR-9, and let-7a expression. Hong et al. (21) propose a multicomponent mathematical model for simulating lung cancer growth as well as radiotherapy treatment for lung cancer, showing promising predictive accuracy compared to a relatively small set of *in vivo* data points.

Unfortunately, current PET-CT technology lacks the ability to clearly capture small metastasis, usually less than 2 mm in diameter due to the mix of cancer and healthy cells together with the noise occurring during the sampling process (22). Missing small-size metastasis can lead to choosing the sub-optimal course of treatment and result in clinically catastrophic results. In this work, we propose a bio-physical model to predict from PET-CT imagery the locations of small-size metastasis that the current PET-CT methods are missing. Data-driven models are increasingly being utilized in the field of oncology (23, 24). By utilizing patient-specific biological and clinical data, these models aim to provide a more comprehensive representation of the disease and its progression, thereby enabling more targeted and effective treatment strategies (25, 26). The use of these models in the treatment of lung cancer holds great promise, and this study aims to evaluate their ability to predict the location of lung cancer metastases, with the ultimate goal of improving patient outcomes (27).

The novelty of this work lies in the combination of three types of bio-physical models associated with cancer settlement, flow in the bloodstream, and growth inside healthy tissue. We tested the proposed model on the historical data of 10 lung cancer patients with metastasis, obtaining a 74% accuracy in the prediction of the metastasis locations.

The remainder of the paper is organized as follows. Section 2 outlines the proposed bioclinical model, divided into the biophysical model, initial condition construction from the 3D CT image, and the metastasis probability heat-map generation process. Section 3 presents the performance of the proposed model on real-world clinical data. Finally, section 4 discusses the obtained results with their clinical applications and proposes possible future work.

2 Methods

The spread dynamics of metastasis originating in the primary tumor can be associated with three main biological processes: (1) the flow of cancer cells in the bloodstream; (2) the settlement of cancer cells in the tissue; and 3) the spatial spread of cancer polyps (28–30). All these biological processes are spatio-temporal

in nature and therefore influenced by the spatial distributions of blood vessels, healthy tissue, and the original cancer cells. To capture these settings, we use a chest PET-CT image, obtaining a three-dimensional (3D) gray-scale image ($I \in \mathbb{R}^{x \times y \times z}$) where x, y, z are the CT image's dimensions. Using I, and by simulating the biological and clinical occurring *in vivo*, one can predict the locations of cancer's metastasis, if these exist. A schematic view of the model's components and the interactions between them is summarized in Figure 1. Namely, the algorithm can be divided into three main components. First, biophysical modeling is responsible for predicting the ability of cancer cells to colonize different parts of the lungs over time. Second, the computer vision algorithm accepts the 3D CT image and produces the parameterized initial condition construction for the biophysical model. Finally, an algorithm that utilizes the biophysical model to generate the metastasis heatmap.

2.1 Biophysical modeling

To capture the biological processes occurring *in vivo* in a patient's lungs in the context of lung cancer migration, we define a model, M. Formally, M is a function $M : \mathbb{G} \times \mathbb{R}^3 \times \{0, 1\}^{x \times y \times z} \times \mathbb{R}^3 \to \mathbb{R}^+$ such that $M(G, p[l], I, \tau) \to c$, where $G \in \mathbb{G}$ is the flow graph, $p[l] \in \mathbb{R}^3$ is the location of the primary tumor in the image I, and $I \in \{0, 1\}^{x \times y \times z}$ is a 3D binary image with 1 for locations where cancer cells can settle and 0 otherwise, $\tau \in \mathbb{R}^3$ is the location of interest to evaluate in the image I, and $c \in \mathbb{N}$ is the total number of cancer cells predicted to settle in location τ.

Formally, the model operates as follows. First, we find the blood vessel $b_s \in B_s$ that is closest to the primary tumor location ($p[l]$) by computing the distance between the primary tumor location and each blood vessel $\forall b_s \in B_s$ and taking the minimal value. Afterward, in the same manner, the blood vessel closest to $\bar{x}$. These two locations are marked by $\bar{S} \in b_s^S$ and $\bar{T} \in b_s^T$, respectively. Afterward, we find all the paths in the flow graph (G) shorter than a length ν such that starts at b_s^S and ends at b_s^T using the breadth-first search (BFS) algorithm (31).

It is known that the cancer cell population's size is reducing exponentially over time (32, 33). Hence, if the absolute value of cancer cells in the cardiovascular is less than a pre-defined threshold $\xi \in \mathbb{N}$, the population size is set to be zero and by that defines the value of ν and the stop condition for this step in the model.

Hence, we proposed a prediction algorithm A that gets as an input the location of a primary tumor τ_l and its size τ_s, the blood vessels, and the connections between them as a graph $G = (B, E)$, and a binary 3D tensor of healthy tissue cancer metastasis can colonize and returns a 3D tensor indicating the normalized probability that metastasis would take occur in each segment of the lungs. Namely, one can define algorithm A as follows: $A : \mathbb{R}^{x \cdot y \cdot z} \times \mathbb{R}^3 \times \mathbb{R} \to \mathbb{R}^{x \cdot y \cdot z}$ such that $A(I, \tau_l, \tau_s) \to P(I)$, where $I \in \mathbb{R}^{x \cdot y \cdot z}$ is the CT image, $\tau_l \in \mathbb{R}^3$ is the location of the prime tumor in I, $\tau_s \in \mathbb{R}$ is the size of the primary tumor, and $P(I) \subset \mathbb{R}^{x \cdot y \cdot z}$ is a distribution function allocating a probability of metastasis occurrence for each location in I.

A operates as follows, starting from the primary tumor, the tumor grows according to the model proposed by Newton et al. (34)

FIGURE 1
A schematic view of the model's components and the interactions between them.
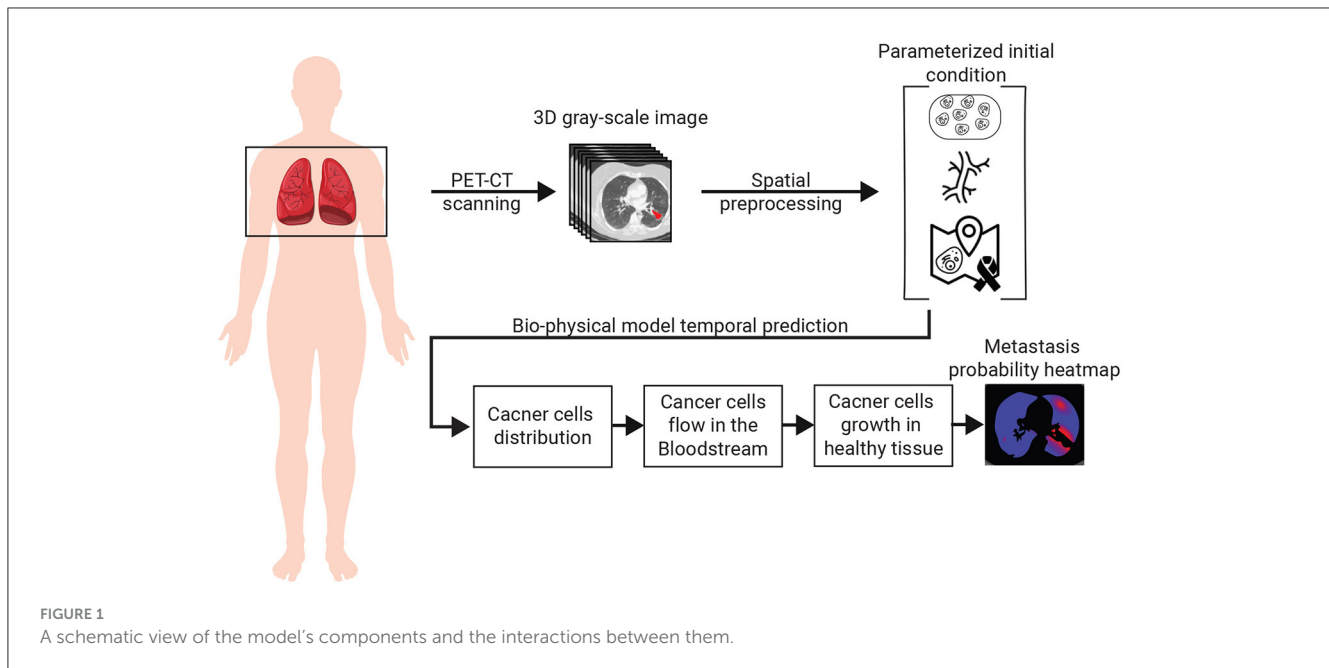
until it reaches a blood vessel. At this point, cancer cells are assumed to drop from the tumor into the bloodstream at some rate $d \in \mathbb{R}^+$. The cancer cells are floating in the bloodstream according to the model proposed by Lazebnik et al. (35). In a probabilistic manner, cancer cells leave the bloodstream toward the tissues around the blood vessels and try to grow into a metastasis. This colonization process is governed by the model proposed by Szomolay et al. (36).

2.2 Initial condition construction

To utilize the proposed bio-physical with an inputted PET-CT 3D image, one first needs to process the image to the required parameterized format that can be used as an initial condition for the model. Namely, it is required to extract the location and size of the primary tumor, the blood vessels in the geometry, and the locations of healthy tissue the cancer cells can colonize.

The first task can be achieved with relatively high accuracy using the method proposed by Miah and Yousuf (37), extracting its location ($\tau_l \in \mathbb{R}^3$) and size $\tau_s \in \mathbb{R}$ in I.

Next, the blood vessels are defined using a graph $G = (B, E)$ such that $E \subset B \times B$. The blood vessels graph, G, is obtained as follows. First, a search radius $R \in \mathbb{R} > 0$ is initialized manually by the user to be R_0. The blood vessels approximated by a cylinder geometry from a 3D CT image are obtained using the algorithm proposed by (38). We denoted the set of blood vessels to be B where $b \in B : b := (c, h, r, o_{xy}, o_{xz})$ such that $c \in \mathbb{R}^3$ is the blood vessel's center of mass, $h \in \mathbb{R}$ is the height of the blood vessel, $r \in \mathbb{R}$ is the average radius of the blood vessel, $o_{xy} \in [0, 2\pi]$ is the orientation in the xy axis, and $o_{xz} \in [0, \pi]$ is the orientation in the xz axis. For convenience, we treat B as a list that is sorted according to the

h parameter, which can be obtained in $O(|B|log(|B|))$ operations using Quicksort algorithm (39). For each $b \in B$, we compute $sl := c - h/2[cos(o_{xy}), cos(\pi/4 - o_{xy}), cos(o_{xz})]$ and $el := c + h/2[cos(o_{xy}), cos(\pi/4 - o_{xy}), cos(o_{xz})]$ which stands for the start and end locations of a cylinder blood vessel, respectively. To contract G, we first initialize it such that B are the nodes and E is an empty edge set. Now, interactively, we add edges to E with the following logic: each blood vessel, $b \in B$ is checked if its start, sl, is inside a 3D sphere defined by the search radius R with either the beginning or end location of another blood vessel. If so, we add it to the edge set, E, such that its end is connected to the closest blood vessel $b \in B$ in terms of $||b_{sl}^i - b_{el}^j||$ where $b^i, b_j \in B \wedge b^i \neq b_j$. If no edge is added, the search radius, R, is increased according to the formula $R \leftarrow R + \delta_R$ such that $\delta_R \in \mathbb{R}^+$ is a pre-define hyperparameter. Once G becomes a connected graph, the process holds. This is because it is biologically known that the cardiovascular system is connected and as such, once this criterion is met, it is assumed the graph is properly constructed. Finally. we compute the maximum (in the manner of radius) spanning tree of the graph G using the method proposed by Al Mamun and Rajasekaran (40).

Finally, the 3D image is first divided into 2D images. Then, the location of the healthy tissue is obtained by using a threshold-adaptive Canny algorithm (41) to first find the edges between the inner part of the lungs and the outer one, alongside other edges in the image that are noise. To remove the unwanted edges, we used Hough Transform (42) to detect two ellipsoids from the edges that approximate the outer divide edges. Afterward, the edges connected to the ones obtained from the Hough Transform's ellipsoids, are added until a close polygon is obtained. The inner side of these two shapes is defined to be the healthy tissue area. After the two shapes are obtained for each 2D image, we reconstruct the entire 3D shape using the Laplacian smoothing method (43).

TABLE 1 The patient's socio-demographic distribution.

Patient	Age	Gender	Smoking status
1	51	M	Yes
2	62	F	No
3	68	M	Yes
4	43	F	Yes
5	52	F	Yes
6	65	F	No
7	57	M	Yes
8	38	F	Yes
9	71	F	Yes
10	63	F	Yes

TABLE 2 The proposed model's performance in terms of the hard- and soft-classifier, divided into patients.

Patient	Hard-classifier score	Soft-classifier score
1	0.782	0.803
2	0.830	0.838
3	0.689	0.706
4	0.656	0.663
5	0.735	0.742
6	0.835	0.851
7	0.721	0.733
8	0.674	0.691
9	0.701	0.714
10	0.690	0.708
MEAN ± STD	0.7313 ± 0.0192	0.7449 ± 0.0193

2.3 Metastasis heatmap generation

Hypothetically, one could solve the heatmap generation as a regression task, solving the model numerically with a given initial condition at time $t_0 \in \mathbb{R}$ and extracting the state of the model at any desired time, $t_f > t_0$. However, as shown in (35), computing such a dynamical system numerically is both computationally expensive and unstable. The main issue lies in the graph-based Navier-Stokes equations (44) one needs to solve. As such, to tackle this challenge, we generate the metastasis heatmap as follows. An 3D binary (I) is uniformly sampled with a grid Ω of size $\alpha_x, \alpha_y, \alpha_z \in \mathbb{N}$ for the x, y, z axes, respectively. The probability of metastasis occurrence in each point in Ω is obtained by solving the biophysical model (see Section 2.1) with the initial condition (see Section 2.2) with one modification. The blood flow component is computed for only the path in G from the initial tumor location and the tested point in the grid. Once all points in the grid are tested and the amount of cancer cells is computed for a pre-defined stop time $T \in \mathbb{R}^+$, the values are normalized using the L_1 metric to define probability.

3 Results

To evaluate the performance of the proposed bioclinical model, we used samples from 10 patients. All patients are diagnosed with metastases in the lungs in the Sheba Hospital (Israel) between 2019 and 2022. The metastasis instances have been manually tagged by a clinician, indicating the location in the lung and the size, alongside a manual tagging of the prime tumor's location and size. For these patients, a CT image before the detection of metastasis and afterward are obtained, without treatment in between, allowing for validation of the metastasis occurring locations without outside influence. Table 1 shows the socio-demographic properties of the cohort.

Table 2 outlines the result of this computation, divided into the Hard and Soft classifier scores. Overall, the bioclinical model shows 74% accuracy, on average, in predicting the location of lung metastasis from lung cancer with a 1.9% standard deviation. This indicates that the model receives stable levels of performance over the sampled population. The scores describe the accuracy metric

of a Soft-classifier between two 3D images $I_1 \in \{0, 1\}^{x \cdot y \cdot z}$ and $I_2 \in \mathbb{R}^{x \cdot y \cdot z}$ where I_1 is a binary image that indicates if a cell in the image is part of a cancer polyp or not and I_2 is the prediction of the proposed model (see Section 2.3):

$$d_s(I_1, I_2) := 1 - \frac{\sum_{1 \le i \le x} \sum_{1 \le j \le y} \sum_{1 \le k \le z} (I_1[x,y,z] - I_2[x,y,z])^2}{x \cdot y \cdot z}.$$

In addition, we formally define the Hard-classifier score to be $d_h : \{0, 1\}^{x \cdot y \cdot z} \times \{0, 1\}^{x \cdot y \cdot z} \times \mathbb{R} \rightarrow \mathbb{R}$ such that $d_h(I_1, I_2, \zeta) := d_s(I_1, I_2|_\zeta)$ where $I_2|_\zeta$ is obtained by performing a threshold ζ on the predicted image I_2. I.e. each value $\alpha \in I_2$ is replaced with 1 if $\alpha > \zeta$ and 0 otherwise).

One can notice that the standard deviation of both the Hard and Soft classifiers are relatively small (0.0192 and 0.0193, respectively), which indicates that the proposed model is relatively robust for this cohort. Moreover, focusing on the Hard-classifier, the performance ranges from 0.690 to 0.830 which indicates that outside parameters influence the model's performance. That said, age, gender, and smoking status are not directly correlated to the performance based on the obtained cohort.

4 Discussion

The spread of lung cancer from its primary site to other parts of the lungs is a critical aspect of lung cancer progression and is associated with decreased survival rates (45, 46). Early identification of metastatic lesions is crucial for prompt and effective treatment, as it can significantly impact patient outcomes (47). However, conventional imaging techniques such as computed tomography (CT) scans have limitations in detecting small metastases (48, 49). In this study, we proposed a personalized biophysical-based bioclinical mathematical model that accepts a patient's 3D CT image and produces a 3D heatmap of the probability a metastasis would develop in each region of the lungs.

We tested our bioclinical model on real-world clinical data and validated it with clinician domain experts to get a baseline. As seen
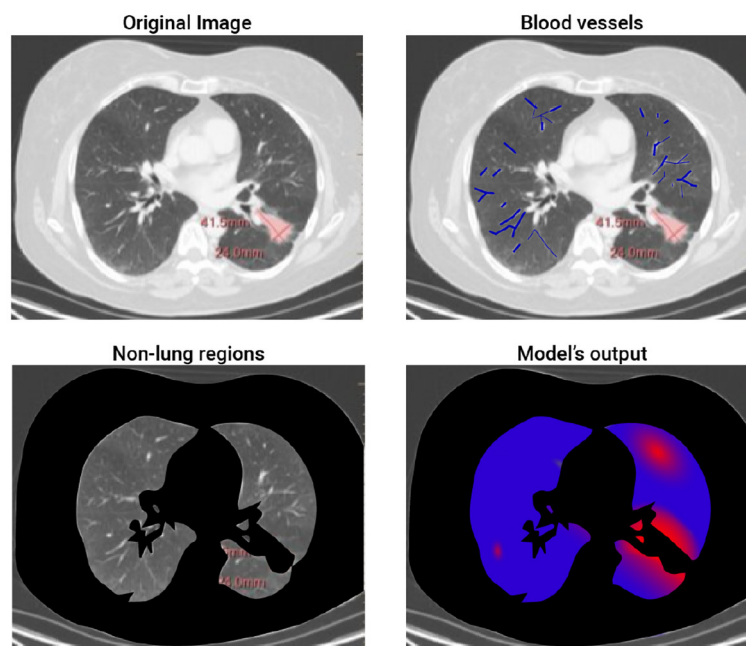
FIGURE 2
A 2D slice of patient #2. The figure shows the four steps of the proposed method. The top-left image is the input image where the red mark is manually tagged (the proposed model is not aware of this tag). The top-right image highlights the blood vessels detected by the model. The bottom-left image highlights (in black) the non-lung regions removed by the proposed model. Finally, the bottom-right image shows the obtained heatmap.

in Table 2, the proposed bioclinical model provides around 74% accuracy in predicting the location of metastasis. This means, that on average, three out of four predictions of the model marked locations with metastasis in the CT that would not be marked otherwise. However, these results do not provide a lower-boundary accuracy measurement of the model's performance as locations marked by the algorithm with metastasis that was without are either a wrong prediction or that metastasis was not found during the validation phase and would be created given more time. For example, let us examine a 2D slice of one of the patients in the sample. Figure 2 shows the original CT image slice (with the manual mark of the primary tumor), the blood vessels marked in blue, the healthy tissue locations, and the model's heatmap prediction - from left to right and top to bottom. One can notice that the model predicts metastasis for the right-top corner of the lungs in this z-axis value. However, metastasis is not found there. This is because either the model is mistaken or not enough time passed from the first and second CT scans in order to allow metastasis to grow into a detected size.

One of the key advantages of the bioclinical model is the fact it is based on biophysical modeling of the cancer spread which allows one to integrate diverse data sources and provides a more comprehensive understanding of the disease compared to purely data-driven methods. Theoretically, one could aim to develop a data-driven solution to this time-series task using ML or deep learning methods. However, to do so, an extensive data-gathering process of multiple CT scans of lung cancer would be required, which would be extremely expensive, logistically complex, and ethically questionable. On the other hand, the proposed approach utilizes previous biological, physical, and clinical knowledge, resulting in a need for just a relatively small dataset, used entirely to validate and evaluate the performance of the proposed model.

The results of this study demonstrate the potential of mathematical models in predicting the location of lung cancer metastases. Our findings show that the bioclinical model can provide personalized predictions of metastatic spread with decent accuracy. Hence, this model can potentially inform more targeted and effective treatment strategies for lung cancer patients, ultimately improving patient outcomes. As such, this study provides a step forward in developing more personalized and effective treatments for lung cancer. The use of bio-clinical mathematical models to predict the location of metastases holds great promise for improving patient outcomes and should be a focus of future research efforts in this field.

However, our bioclinical model can (and should) be further improved. First, the currently used biomathematical model of cancer colonization on healthy tissue does not take into consideration the spatial properties of the cancer cells. Second, cancer cells continue to mutate over time which causes a wide range of outcomes and can significantly alter the course of metastasis formation. Third, taking into consideration additional clinical data about the patient such as gender, background diseases, smoking, and others, it will be possible to obtain more accurate the location of cancer metastases (50). Forth, this study was limited by its sample size (of 10 patients) and the heterogeneity of the patient population. Thus, additional large-scale, multicentered trials are necessary to further test the accuracy and clinical utility of the proposed model, to obtain more statistically representative results. In addition, as

future work, molecular dynamics simulations can be also integrated into the proposed model to further improve its accuracy (51).

Taken jointly, the proposed bioclinical model provides a new perspective of the metastasis location appearance for lung cancer using PET-CT data. This model can be medically useful for patients with stage two lung cancer where it is not clear from the PET-CT image itself if metastasis already occurred and is too small to detect or has not occurred yet by highlighting potential locations in the image for medical experts, allowing a later medical decision process with better information. Nonetheless, further research should be made to validate the obtained results on a larger cohort to statistically establish its usefulness.

Data availability statement

The raw data supporting the conclusions of this article will be made available by the authors, without undue reservation.

Author contributions

TL: Conceptualization, Formal analysis, Funding acquisition, Investigation, Methodology, Project administration, Resources, Software, Visualization, Writing – original draft, Writing – review & editing. SB-M: Data curation, Writing – original draft, Writing – review & editing.

Conflict of interest

The authors declare that the research was conducted in the absence of any commercial or financial relationships that could be construed as a potential conflict of interest.

Publisher's note

All claims expressed in this article are solely those of the authors and do not necessarily represent those of their affiliated organizations, or those of the publisher, the editors and the reviewers. Any product that may be evaluated in this article, or claim that may be made by its manufacturer, is not guaranteed or endorsed by the publisher.

References

1. Torre LA, Siegel RL, Jemal A. Lung cancer statistics. *Adv Exp Med Biol*. (2016) 893:1–19. doi: 10.1007/978-3-319-24223-1_1

2. Yuan M, Huang LL, Chen JH, Wu J, Xu Q. The emerging treatment landscape of targeted therapy in non-small-cell lung cancer. *Signal Transduct Target Ther*. (2019) 4:61. doi: 10.1038/s41392-019-0099-9

3. Reck M, Popat S, Reinmuth N, De Ruysscher D, Kerr KM, Peters S. Metastatic non-small-cell lung cancer (NSCLC): ESMO Clinical Practice Guidelines for diagnosis, treatment and follow-up. *Ann Oncol*. (2014). 25:III27–39. doi: 10.1093/annonc/mdu199

4. Wang M, Herbst RS, Boshoff C. Toward personalized treatment approaches for non-small-cell lung cancer. *Nat Med*. (2021) 27:1345–56. doi: 10.1038/s41591-021-01450-2

5. Popper HH. Progression and metastasis of lung cancer. *Cancer Metast Rev*. (2016) 35:75–91. doi: 10.1007/s10555-016-9618-0

6. Ambrosini V, Nicolini S, Caroli P, Nanni C, Massaro A, Cristina MM, et al. PET/CT imaging in different types of lung cancer: an overview. *Eur J Radiol*. (2012) 81:988–1001. doi: 10.1016/j.ejrad.2011.03.020

7. Evangelista L, Cuocolo A, Pace L, Mansi L, Del Vecchio S, Miletto P, et al. Performance of FDG-PET/CT in solitary pulmonary nodule based on pre-test likelihood of malignancy: results from the ITALIAN retrospective multicenter trial. *Eur J Nucl Med Mol Imag*. (2018) 45:1898–907. doi: 10.1007/s00259-018-4016-1

8. He YQ, Gong HL, Deng YF Li WM. Diagnostic efficacy of PET and PET/CT for recurrent lung cancer: a meta-analysis. *Acta Radiol*. (2014) 55:309–17. doi: 10.1177/0284185113498536

9. Hochhegger B, Alves GRT, Irion KL, Fritscher CC, Fritscher LG, Concatto NH, et al. PET/CT imaging in lung cancer: indications and findings. *Jornal Brasileiro de Pneumologia*. (2015) 41:4479. doi: 10.1590/S1806-37132015000004479

10. Spadafora M, Evangelista L, Fiordoro S, Pircaro F, Sicignano M, Mansi L. The multicenter ITALIAN trial assess the performance of FDG-PET/CT related to pre-test cancer risk in patients with solitary pulmonary nodules and introduces a segmental thoracic diagnostic strategy. *Curr Radiopharmaceut*. (2020) 13:243–8. doi: 10.2174/1874471013666200318142210

11. Lakshmanaprabu SK, Sachi NM, Shankar K, Arunkumar N, Gustavo R. Optimal deep learning model for classification of lung cancer on CT images. *Future Generat Comp Syst*. (2019) 92:374–82. doi: 10.1016/j.future.2018.10.009

12. Guo Z, Xu L, Si Y, Razmjooy N. Novel computer-aided lung cancer detection based on convolutional neural network-based and feature-based classifiers using metaheuristics. *Int J Imaging Syst Technol*. (2021) 31:1954–69. doi: 10.1002/ima.22608

13. Savchenko E, Lazebnik T. Computer aided functional style identification and correction in modern Russian texts. *J Data, Informat Manage*. (2022) 4:25–32. doi: 10.1007/s42488-021-00062-2

14. Tandon R, Agrawal S, Chang A, Band SS. Hybrid deep learning model for detection and classification of lung carcinoma using chest radiographs. *Front Public Health*. (2022) 894920:1–13. doi: 10.3389/fpubh.2022.894920

15. Lazebnik T. Cell-level spatio-temporal model for a bacillus calmette-guérin-based immunotherapy treatment protocol of superficial bladder cancer. *Cells*. (2022) 11:2372. doi: 10.3390/cells11152372

16. Umar M, Sabir Z, Amin JLG F. Guirao, Raja MAZ. Stochastic numerical technique for solving HIV infection model of CD4+ T cells. *Eur Phys J Plus*. (2020) 135:403. doi: 10.1140/epjp/s13360-020-00417-5

17. De Pillis LG, Gu W, Radunskaya AE. Mixed immunotherapy and chemotherapy of tumors: modeling, applications and biological interpretations. *J Theor Biol*. (2006) 238:841–62. doi: 10.1016/j.jtbi.2005.06.037

18. Eikenberry S, Thalhauser C, Kuang Y. Tumor-immune interaction, surgical treatment, and cancer recurrence in a mathematical model of melanoma. *PLoS Comp Biol*. (2009) 5:e1000362. doi: 10.1371/journal.pcbi.1000362

19. Louzoun Y, Xue C, Lesinski GB, Friedman A. A mathematical model for pancreatic cancer growth and treatments. *J Theor Biol*. (2014) 351:74–82. doi: 10.1016/j.jtbi.2014.02.028

20. Kang HW, Crawford M, Fabbri M, Nuovo G, Garofalo M, Nana-Sinkam SP, et al. A mathematical model for microRNA in lung cancer. *PLoS ONE*. (2013) 8:1–19. doi: 10.1371/journal.pone.0053663

21. Hong WS, Wang SQ, Zhang GQ. Lung cancer radiotherapy: simulation and analysis based on a multicomponent mathematical model. *Comput Math Methods Med*. (2021) 2021:6640051. doi: 10.1155/2021/6640051

22. Wang P, DeNunzio A, Okunieff P, O'Dell WG. Lung metastases detection in CT images using 3D template matching. *Med Phys*. (2007) 34:915–22. doi: 10.1118/1.2436970

23. Lazebnik T, Bahouth Z, Bunimovich-Mendrazitsky S, Halachmi S. Predicting acute kidney injury following open partial nephrectomy treatment using SAT-pruned explainable machine learning model. *BMC Med Inform Decis Mak*. (2022) 22:133–40. doi: 10.1186/s12911-022-01877-8

24. Yu X, Ji Y, Huang M, Feng Z. Machine learning for acute kidney injury: changing the traditional disease prediction mode. *Front Med*. (2023). 10:1–21. doi: 10.3389/fmed.2023.1050255

25. Moreira AL, Eng J. Personalized therapy for lung cancer. *Chest*. (2014) 146:1649–57. doi: 10.1378/chest.14-0713

26. Pakkala S, Ramalingam SS. Personalized therapy for lung cancer: striking a moving target. *JCI Insight*. (2018) 3:e120858. doi: 10.1172/jci.insight.120858

27. Kim SM, Lee H, Min BH, Kim JJ, An JY, Choi MG, et al. A prediction model for lymph node metastasis in early-stage gastric cancer: toward tailored lymphadenectomy. *J Surg Oncol*. (2019) 120:670–5. doi: 10.1002/jso.25628

28. Larsen JE, Minna JD. Molecular biology of lung cancer: clinical implications. *Clin Chest Med*. (2011) 32:703–40. doi: 10.1016/j.ccm.2011.08.003

29. Lambert AW, Pattabiraman DR, Weinberg RA. Emerging biological principles of metastasis. *Cell*. (2017) 168:670–91. doi: 10.1016/j.cell.2016.11.037

30. Fidler IJ. Tumor heterogeneity and the biology of cancer invasion and metastasis1. *Cancer Res*. (1978) 38:2651–60.

31. Zhu YT, Cheung Y. A new distributed breadth-first-search algorithm. *Inform Process Lett*. (1987) 25:329–33. doi: 10.1016/0020-0190(87)90208-0

32. Ben-Akiva E, Meyer RA, Yu H, Smith JT, Pardoll DM, Green JJ. Biomimetic anisotropic polymeric nanoparticles coated with red blood cell membranes for enhanced circulation and toxin removal. *Sci Adv*. (2020) 6:aay9035. doi: 10.1126/sciadv.aay9035

33. Lee MJE, Veiseh O, Bhattarai N, Sun C, Hansen SJ, Ditzler S, et al. Rapid pharmacokinetic and biodistribution studies using cholorotoxin-conjugated iron oxide nanoparticles: a novel non-radioactive method. *PLoS ONE*. (2010) 5:e9536. doi: 10.1371/journal.pone.0009536

34. Newton PK, Mason j, Bethel K, Bazhenova LA, Nieva J, Kuhn P. A stochastic markov chain model to describe lung cancer growth and metastasis. *PLoS ONE*. (2012) 7:1–18. doi: 10.1371/journal.pone.0034637

35. Lazebnik T, Weitman H, Kaminka GA. Generic purpose pharmacokinetics-pharmacodynamics mathematical model for nanomedicine targeted drug delivery: mouse model. *bioRxiv*. (2022). doi: 10.1101/2022.07.13.499855

36. Szomolay B, Eubank TD, Roberts RD, Marsh CB, Friedman A. Modeling the inhibition of breast cancer growth by GM-CSF. *J Theoret Biol*. 303:141–51. doi: 10.1016/j.jtbi.2012.03.024

37. Miah BA, Yousuf MA. Detection of lung cancer from CT image using image processing and neural network. In: *2015 International Conference on Electrical Engineering and Information Communication Technology (ICEEICT)*. Savar: IEEE (2015). p. 1–6. doi: 10.1109/ICEEICT.2015.7307530

38. Kirbas C, Quek FKH. Vessel extraction techniques and algorithms: a survey. In: *Third IEEE Symposium on Bioinformatics and Bioengineering, 2003 Proceedings*. Bethesda, MD: IEEE (2003). p. 238–45.

39. Hoare CAR. Quicksort. *Comp J*. (1962) 5:10–6. doi: 10.1093/comjnl/5.1.10

40. Al Mamun A, Rajasekaran S. An efficient Minimum Spanning Tree algorithm. In: *2016 IEEE Symposium on Computers and Communication (ISCC)*. Messina: IEEE (2016). p. 1047–52. doi: 10.1109/ISCC.2016.7543874

41. Canny J. A computational approach to edge detection. *IEEE Trans Pattern Anal Mach Intell*. (1986) 6:679–98. doi: 10.1109/TPAMI.1986.4767851

42. Duda RO, Hart PE. Use of the Hough transformation to detect lines and curves in pictures. *Commun ACM*. (1972) 15:11–5. doi: 10.1145/361237.361242

43. Volodine T, Vanderstraeten D, Roose D. Smoothing of Meshes and Point Clouds Using Weighted Geometry-Aware Bases. In: Kim MS, Shimada K, editors. *Geometric Modeling and Processing - GMP 2006*. (2006). p. 687-693. doi: 10.1007/11802914_57

44. Canic S, Mikelic A, Tambaca J, A. two-dimensional effective model describing fluid-structure interaction in blood flow: analysis, simulation and experimental validation. *Comptes Rendus Mecanique*. (2005) 333:867–83. doi: 10.1016/j.crme.2005.10.005

45. Wood SL, Pernemalm M, Crosbie PA, Whetton AD. The role of the tumor-microenvironment in lung cancer-metastasis and its relationship to potential therapeutic targets. *Cancer Treatm Rev*. (2014) 40:558–66. doi: 10.1016/j.ctrv.2013.10.001

46. Asamura H, Goya T, Koshiishi Y, Sohara Y, Eguchi K, Mori M, et al. A japanese lung cancer registry study: prognosis of 13,010 resected lung cancers. *J Thoracic Oncol*. (2008) 3:46–52. doi: 10.1097/JTO.0b013e31815e8577

47. Alix-Panabieres C, Magliocco A, Cortes-Hernandez LE, Eslami-S Z, Franklin D, Messina JL. Detection of cancer metastasis: past, present and future. *Clin Exp Metastasis*. (2022) 39:21–8. doi: 10.1007/s10585-021-10088-w

48. Hochman G, Shacham-Shmueli E, Raskin SP, Heymann E, Bunimovich-Mendrazitsky S. Metastases growth patterns in vivo-a unique test case of a metastatic colorectal cancer patient. *Front Appl Math Stat*. (2019) 5:56. doi: 10.3389/fams.2019.00056

49. Hochman G, Shacham-Shmueli E, Raskin SP, Rosenbaum S, Bunimovich-Mendrazitsky S. Metastasis initiation precedes detection of primary cancer-analysis of metastasis growth *in vivo* in a colorectal cancer test case. *Front Physiol*. (2020) 33391005:1–9. doi: 10.3389/fphys.2020.533101

50. Savchenko E, Rosenfeld A, Bunimovich-Mendrazitsky S. Mathematical modeling of BCG-based bladder cancer treatment using socio-demographics. *Sci Rep*. (2023) 13:18754. doi: 10.1038/s41598-023-45581-7

51. Binder K, Horbach J, Kob W, Paul W, Varnik F. Molecular dynamics simulations. *J Phys: Conden Matter*. (2004) 16:6. doi: 10.1088/0953-8984/16/5/006